Influence of the temperature on growth by ammonia source molecular beam epitaxy of wurtzite phase ScAlN alloy on GaN

Caroline Elias, Maud Nemoz, Hélène Rotella, Frédéric Georgi, Stéphane Vézian, Yvon Cordier, Maxime Hugues

APL Materials

Influence of the temperature on growth by ammonia source molecular beam epitaxy of wurtzite phase ScAlN alloy on GaN

Cite as: APL Mater. **11**, 031105 (2023); https://doi.org/10.1063/5.0139588
Submitted: 21 December 2022 • Accepted: 24 February 2023 • Published Online: 14 March 2023

Caroline Elias, Maud Nemoz, Hélène Rotella, et al.

Influence of the temperature on growth by ammonia source molecular beam epitaxy of wurtzite phase ScAlN alloy on GaN

Cite as: APL Mater. 11, 031105 (2023); doi: 10.1063/5.0139588
Submitted: 21 December 2022 • Accepted: 24 February 2023 •
Published Online: 14 March 2023

Caroline Elias,[1,a] Maud Nemoz,[1] Hélène Rotella,[1] Frédéric Georgi,[2] Stéphane Vézian,[1] Maxime Hugues,[1] and Yvon Cordier[1]

AFFILIATIONS

[1] University Côte d'Azur, CNRS, CRHEA, rue B. Gregory, 06560 Valbonne, France
[2] MINES PARIS, PSL University, Center for Material Forming (CEMEF), UMR CNRS, 06904 Sophia Antipolis, France

[a] Author to whom correspondence should be addressed: cel@crhea.cnrs.fr

ABSTRACT

Due to its large piezoelectric and spontaneous polarization coefficients combined with the possibility of being grown lattice-matched with GaN, wide bandgap ScAlN is becoming a promising material in III-nitride semiconductor technology. In this work, and for the first time, ScAlN growth has been performed by molecular beam epitaxy with ammonia source as nitrogen precursor. High electron mobility transistor heterostructures with a 26 nm thick $Sc_{0.15}Al_{0.85}N$ barrier have been grown on GaN-on-sapphire substrates. The effect of growth temperature, ranging between 620 and 800 °C, was carefully investigated. A smooth surface morphology with a mean roughness below 0.5 nm is obtained whatever the temperature while for 670 °C the (0002) and (10$\bar{1}$3) x-ray diffraction rocking curves show minimum full-width at half-maximum of 620 and 720 arc sec, respectively. Furthermore, two-dimensional electron gases with a high density of 3-3.5 × 10^{13}/cm^2 were evidenced in the heterostructures grown below 720 °C.

I. INTRODUCTION

Wide bandgap semiconductors like III-nitrides InN, GaN, AlN, and their alloys (AlGaN, InAlN, InGaN...) have enabled a large diversity of applications like visible and ultraviolet (UV) light emitting diodes (LEDs) and laser diodes (LDs)[1–3] and high electron mobility transistors (HEMTs) for RF power amplifiers and power switching.[4,5] HEMTs based on AlGaN/GaN heterostructures have been largely developed during the last 20 years reaching industrial level nowadays. However, despite this success, the continuous increase of the device performances required by the application needs is facing limitations, mainly related to the properties of the AlGaN/GaN heterostructure. In particular, the carrier density achievable in the transistor channel determines critical performances such as maximum drain current and operation frequency. In AlGaN/GaN HEMTs, the carriers accumulate in a two-dimensional electron gas (2DEG) formed at the interface due to the bandgap discontinuity and the difference in spontaneous and piezoelectric polarizations.[6,7] Reducing the thickness of the barrier separating the gate from the channel allows us to prevent short-channel effects from appearing when the gate length is decreased to improve high frequency performances.[8] However, the reduction of the barrier thickness induces a strong decrease in the carrier concentration. To counterbalance this effect, a high Al content is required in the AlGaN alloy, ultimately to be replaced by AlN, but at the expense of a larger mismatch strain[9] and thus a higher risk of defects such as microcracks or dislocations generation. To tackle these limitations, the use of scandium aluminum nitride (ScAlN) alloy as a barrier material has been proposed.[10,11] $Sc_xAl_{1-x}N$ is a wide bandgap material with even larger piezoelectric and spontaneous polarization coefficients,[12,13] which ensures a very high charge density at the interface between ScAlN and GaN.[11] Moreover, the $Sc_xAl_{1-x}N$ alloy with x = 0.18 can be grown strain-free (lattice-matched) on GaN, as an InAlN barrier layer,[14] but with a much higher sheet electron concentration at the interface.[11] Therefore, ScAlN is currently a promising barrier layer candidate for building the next generation of high-frequency and high-power HEMTs. For that purpose, the epitaxial growth of ScAlN has been developed recently by few groups

using plasma-assisted molecular beam epitaxy (PA-MBE).[15–17] The growth of ScAlN using metal–organic chemical vapor deposition (MOCVD) is even more challenging due to the crucial choice of the precursors and the need to "rebuild" the reactor to allow Sc incorporation into AlN. The use of Cp3Sc and the heating of the bubbler and the line at about 150 °C have allowed the first ScAlN alloy growth by MOCVD in 2020.[18,19] Very recently $(MCp)_2ScCl$ has been proposed as a new higher vapor pressure precursor, thus allowing to increase the molar flow but also to improve the electrical and structural properties of the AlScN/GaN heterostructure.[20] Despite its very recent history, the epitaxial growth of ScAlN alloy has already allowed the demonstration of high-performance RF-HEMTs,[21,22] ferroelectric-resistive memory,[23] and surface acoustic wave resonators.[24] The first ScAlN/GaN heterostructures grown by MOCVD has been only published in 2020.[18,19] Despite these promising results, the epitaxial growth of ScAlN on GaN is still in its infancy and necessitates further studies. Despite a few papers reporting on the ammonia-source MBE (NH_3-MBE) growth of ScGaN, there is no report about ScAlN up until now. Previous studies on AlGaN/GaN RF-HEMTs obtained by NH_3-MBE allowed to reach high performances.[25–27] Therefore, the growth of ScAlN by such a technique is worth investigating. In this letter, the effect of the growth temperature on the structural and electrical properties of ScAlN/GaN heterostructures grown by NH_3-MBE is studied for the first time. Based on structural and electrical characterization, an optimum growth temperature of around 670 °C has been obtained. For a 26 nm thick ScAlN barrier with 15% Sc content, a 2DEG carrier density of up to $3.5 \times 10^{13}/cm^2$ was deduced from capacitance-voltage (C-V) measurements.

II. EXPERIMENTAL

The samples were grown in a Riber Compact 21 T reactor equipped with effusion cells for gallium, aluminum, and scandium, while ammonia is provided via an injector with a flow rate of 200 sccm.[26] For all the samples, the temperatures of the scandium and the aluminum effusion cells were kept constant at 1200 and 1070 °C, corresponding to beam equivalent pressures of 1.1×10^{-8} and 1.0×10^{-7} Torr, respectively. Commercial MOCVD GaN-on-sapphire templates were used to grow the structures reported on Fig. 1(a). The back side of the templates was coated with 1 μm thick sputtered molybdenum to facilitate the heating and the measurement of growth temperature with an infrared pyrometer. The RF-device GaN HEMTs standard conditions (growth at 800 °C and 200 sccm NH_3 flow rate) have been used to grow the 400–800 nm thick GaN buffer.[28] Thanks to a lower concentration of residual donors, NH_3 growth permits to achieve higher resistivity GaN buffer layer which is critical for HEMT applications.[29] Prior to the barrier growth, a 1 nm thick AlN interlayer is used to reduce the penetration of the 2DEG wave function into the barrier to limit the alloy scattering responsible for electron mobility degradation. Then the ScAlN barrier was grown at a temperature Tg ranging from 620 to 800 °C. In this temperature range, the element III sticking coefficients can be considered constant. Therefore, in such nitrogen-rich conditions (growth pressure around 10^{-5} Torr), we expect the growth rate and thus the alloy composition to be almost independent of growth temperature, which is a noticeable advantage compared to PA-MBE. Reflection high-energy electron diffraction (RHEED) was systematically used to follow the evolution of the surface morphology during the growth.

The elemental composition of ScAlN alloy was determined using X-ray photoelectron spectroscopy (XPS) with an aluminum source and secondary ion mass spectroscopy (SIMS) on dedicated calibration samples. Tapping mode atomic force microscopy (AFM) was used to assess the surface morphology. The crystalline quality of the epitaxial films and especially of the ScAlN barrier was studied using high resolution x-ray diffraction (HRXRD) $2\Theta/\omega$ and ω scans (rocking curves) for symmetric (0002) and asymmetric $(10\bar{1}3)$ reflections. In- and out- of plane lattice parameters were determined using reciprocal space mapping (RSM) at $(10\bar{1}5)$ reflection. The 2DEG density induced at the ScAlN/GaN interface was deduced from C-V measurements performed at 10 kHz with a mercury probe and an Agilent 4284 A LCR meter.

III. RESULTS AND DISCUSSION

The RHEED pattern observed after the barrier growth at 760 °C is shown in Fig. 1(b). This streaky pattern attests to bidimensional growth, and it has been observed without any additional features for samples grown between 670 and 760 °C. For lower growth temperatures, only a slight broadening of the diffraction lines is observed. However, no additional spots announcing the presence of cubic phases have been observed in the growth temperature range studied.

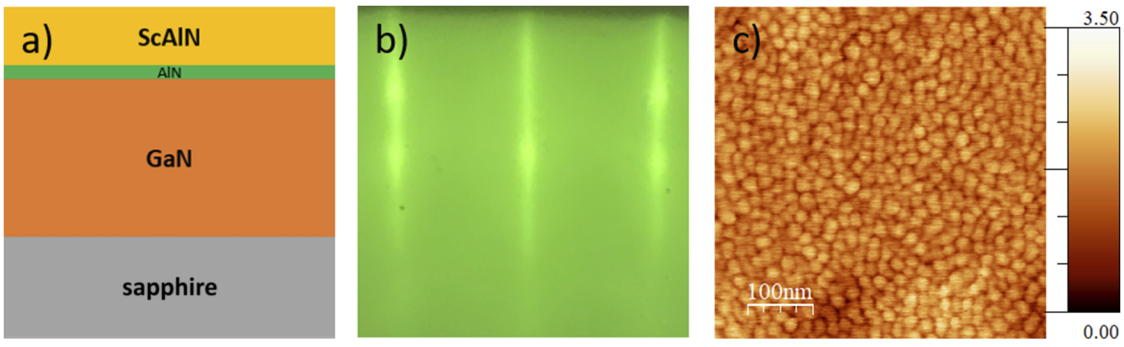

FIG. 1. (a) Epitaxial structure schematic, (b) RHEED pattern, and (c) 500 × 500 nm^2 AFM scan with 0.3 nm of rms roughness for ScAlN grown at Tg = 760 °C.

A similar trend of the RHEED evolution has already been reported for ScAlN grown by PA-MBE.[10]

Atomic force microscopy (AFM) performed on the film grown at 670–760 °C confirms the two-dimensional growth with a root mean square (rms) roughness below 0.4 nm for 500 × 500 nm^2 area scans. As shown in Fig. 1(c), the typical surface morphology for this temperature range consists of homogeneous features with a mean diameter of 20 nm. The periodic height variation resulting from these features can explain the slight intensity modulation observed along the RHEED pattern diffraction lines [Fig. 1(b)]. Despite the different nitrogen source, similar features are also noticed for ScAlN grown by PA-MBE.[15] Out of this temperature range, less homogeneous features are observed. Considering the temperature range studied, a slight increase of the feature diameter with growth temperature is noticed. Furthermore, the rms roughness decreased from 0.43 ± 0.08 to 0.24 ± 0.08 nm as the growth temperature was increased from 620 to 800 °C.

X-ray photoelectron spectroscopy is used to identify the atomic elements present in the films within an analysis depth of 10 nm. It is possible to obtain a composition profile through successive etchings with an argon ion gun. After removing surface pollution and oxide, the atomic composition of the various films is quite stable. The XPS spectrum of the sample grown at 720 °C is shown in Fig. 2(a). The peaks with binding energies of 75, 397, 401, and 405 eV correspond to Al 2p, N1s, Sc 2p$_{3/2}$, and Sc 2p$_{1/2}$, respectively. The relative Sc content in ScAlN was calculated from the Sc2p and Al2p peak areas with the Advantage software, which takes into account the sensitivity factors of each atomic element and corrects the energy-dependent analysis thickness. The ratio of the normalized areas is then used to determine the relative content of Sc, compared to Al, in the ScAlN film. For all samples except the one grown at 670 °C, the relative percentage of Sc is between 15% and 16% [Fig. 2(b)], and a slight decrease in Sc content is observed as the growth temperature increases. The scandium contents in the films were defined as the average of the values obtained at different erosion times, t = 50 s, t = 70 s, and t = 100 s for each sample, which exhibits a fluctuation inferior to 1.5% for each growth temperature. The time necessary for the erosion of the whole ScAlN film is 170 s.

X-ray reflectivity (XRR) has been performed on the sample series to accurately determine the barrier thickness. The XRR spectrum for the sample grown at 670 °C and the corresponding fit obtained using GenX software are shown in Fig. 2(c). Within the accuracy of the fitting procedure, the extracted thicknesses are unchanged for the whole studied temperature range [Fig. 2(d)].[30] The little influence of the growth temperature on the Sc composition and the layer thickness highlights the stable Al and Sc sticking coefficients in this temperature range, resulting in a ScAlN growth rate of 150 nm/h.

The HRXRD 2**Θ**/ω scans of the studied samples are shown in Fig. 3(a). The asymmetry of the GaN peak plotted on a semi-log scale reveals a different strain gradient in some of the templates. However, the position of the GaN peak at 34.5° indicates that the upper part of the templates is fully relaxed with an out-of-plane parameter c = 5.189 Å. The spectra show a second peak around 35.6°,

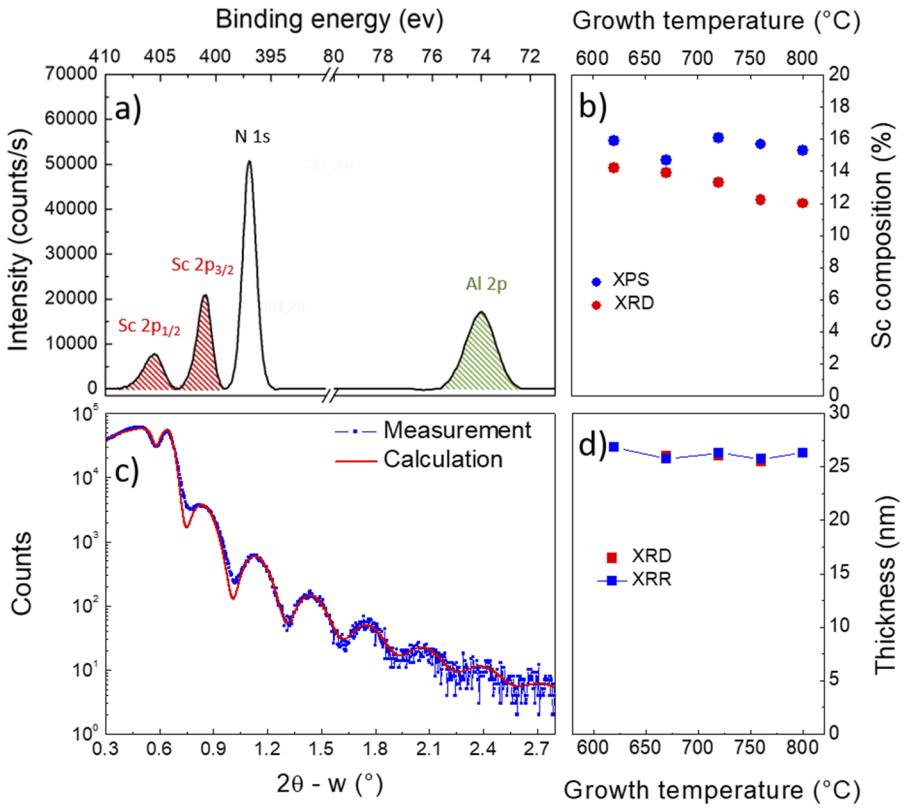

FIG. 2. (a) XPS spectrum of ScAlN sample grown at 670 °C, (b) Sc composition as a function of the growth temperature deduced by XPS (blue) and XRD (red), (c) XRR scan of sample grown at 670 °C experimental (blue) and simulation (red) spectra, and (d) deduced ScAlN barrier thicknesses as a function of the growth temperature.

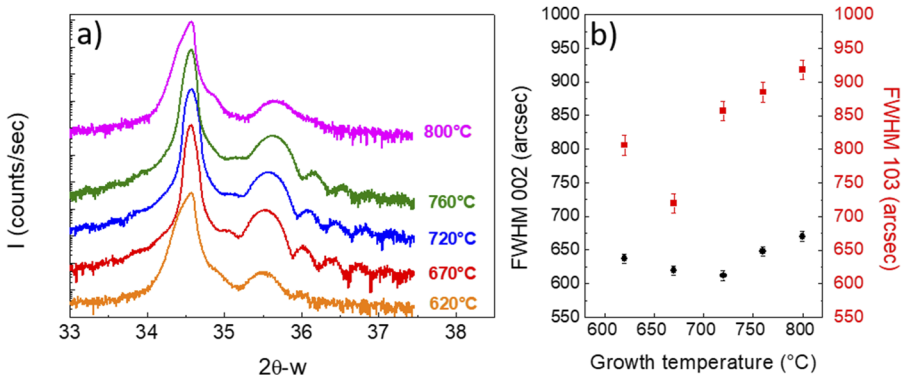

FIG. 3. (a) (0002) plane XRD 2Θ-ω scans and (b) (0002) and (10$\bar{1}$3) ScAlN x-ray rocking curves FWHM as a function of the growth temperature.

accounting for the presence of ScAlN with a single crystalline wurtzite phase. As the growth temperature increases, the ScAlN peak is continuously shifted toward larger angle indicating a small decrease of scandium content, in agreement with XPS measurements [Fig. 2(b)]. A similar trend has been observed within a larger range of temperatures for films grown by PAMBE on GaN.[10,31] In addition, Pendellösung fringes are clearly observed for the films grown between 650 and 740 °C indicating smooth surfaces and interfaces. The barrier thicknesses deduced from the simulation of such fringes using the AMASS software are around 26 nm, comparable to the values obtained by XRR [Fig. 2(d)]. On the other hand, for lower and higher growth temperatures, the fringes disappear. This could be due to a rougher interface and/or deterioration of the crystal quality, or a degradation of the alloy homogeneity, despite the quite homogeneous Sc content deduced from the XPS profiles. Scandium content has been also deduced by simulating HRXRD 2Θ/ω scans, while considering the elastic constants C_{13} and C_{33} reported by Refs. 7,13,32 [see Fig. 2(b)].

To assess the crystal quality, the full width at half maximum (FWHM) of the ω scans has been extracted [Fig. 3(b)]. The FWHM of the (0002) reflection line is lower for Tg = 670 °C (620 arc sec) and Tg = 720 °C (612 arc sec), whereas the FWHM of the (10$\bar{1}$3) reflection line is minimum at 720 arc sec for a Tg = 670 °C. We point out that the FWHM value of the (10$\bar{1}$3) reflection obtained for Tg = 670 °C has been confirmed by several measurements. The beam spot size is around 10 mm. Several measurements of FWHM for (0002) and (10$\bar{1}$3) reflections on different regions of the sample provide a standard deviation of 7 and 14 arc sec, respectively [see Fig. 3(b)]. Furthermore, the (0002) and (10$\bar{1}$3) reflection FWHMs of GaN were very similar for all the samples, around 360 and 430 arc sec, respectively, attesting equivalent template crystal quality with threading dislocation density estimated around 4×10^8 cm^{-2}. Based on the FWHMs, we can conclude that the highest crystalline quality is reached for the ScAlN film grown around 670 °C. Moreover, the evolutions of both the (0002) and (10$\bar{1}$3) FWHMs are consistent with the disappearance of the Pendellösung fringes observed on 2Θ/ω for the lowest and highest temperatures, respectively.

For the sample grown at 670 °C (10$\bar{1}$5), a reflection HRXRD reciprocal space map (not shown here) was performed to determine the in- and out-of-plane lattice parameters of the ScAlN layer and the GaN buffer. Both materials present an identical in-plane lattice parameter of 3.188 Å. The out-of-plane lattice parameters of ScAlN and GaN are equal to 5.048 and 5.189 Å, respectively. The former lattice parameter is in agreement with the one theoretically expected with x = 15%[7] and consistent with XPS results [Fig. 2(b)]. However, like for the InAlN alloy lattice matched on GaN,[33] local strain and/or

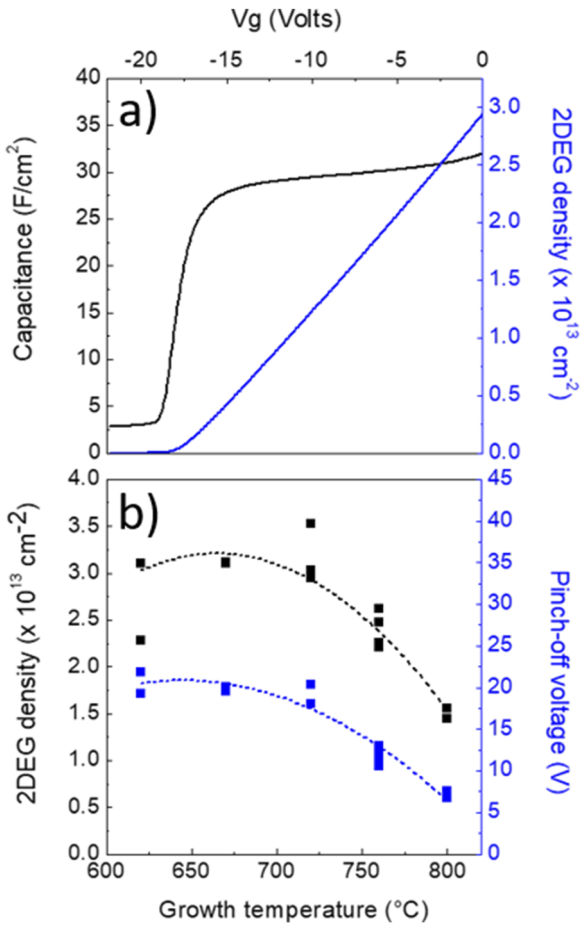

FIG. 4. (a) Capacitance-voltage measurement on ScAlN grown at Tg = 720 °C, (b) 2DEG density and pinch-off voltage as a function of the growth temperature.

compositional fluctuations can develop due to the large differences in bonding energies between AlN and ScN (2.88 and 1.0 eV, respectively, for AlN and ScN). Moreover, as the roughness variation with growth temperature is very limited, it is not likely to explain the observed different crystal quality.

Figure 4(a) shows the capacitance-voltage profile obtained on the HEMT heterostructure with a ScAlN barrier grown at 670 °C. The capacitance plateau attests to the presence of a 2DEG. According to the plateau flatness, a high residual doping level in the barrier is not likely. The measured capacitance is associated with a parallel conductance, and we noticed a systematic increase of the latter while decreasing the growth temperature. This indicates enhanced tunneling through defects within the barrier or at the interface with the mercury probe. The sheet charge concentration (Ns) calculated by integration of the capacitance is between $3.0 \times 10^{13}/cm^2$ and $3.5 \times 10^{13}/cm^2$ for the lower growth temperatures (620 °C up to 720 °C) and suffers a rapid drop-off for higher temperatures [Fig. 4(b)]. Consistently, a concomitant drop in the pinch-off voltage is noticed. According to HRXRD analysis, the optimum growth temperature for the $Sc_{0.15}Al_{0.85}N$ alloy is between 670 and 720 °C with the lowest FWHM for $(10\bar{1}3)$ and (0002) XRD lines, respectively. For this temperature range, the sheet charge concentration (Ns) is maximum and constant, and the parallel conductance analysis indicates that the highest temperature is suitable. Even if the measured sheet charge density is much higher than in AlGaN/GaN and InAlN/GaN systems, the present values are lower than the expected ones reported in Ref. 11. It could be related to the presence of a 2–3 nm thick oxide layer at the surface observed by XPS. Since the surface of the present samples are not passivated, *in situ* passivation with GaN or SiN has to be investigated to reach even better properties.[18]

IV. CONCLUSIONS

The effect of temperature on the quality of thin ScAlN films grown on GaN by ammonia source MBE has been studied. According to our results, a 50 °C growth temperature window (670–720 °C) allows us to reach the highest crystalline wurtzite phase quality for films with smooth interfaces and an in-plane lattice parameter matched with the GaN buffer. This study revealed no significant influence of the growth temperature on either the scandium composition or the barrier thicknesses, which is interesting for a well mastered epitaxy process. These optimizations result in the formation of a 2DEG at the ScAlN/GaN interface with a density up to $3.5 \times 10^{13}/cm^2$, and further studies on highly resistive buffer layers are now to be carried out to specifically assess the transport properties of the 2DEG. Furthermore, even when the obtained carrier density is very promising for the fabrication of high power and high frequency transistors, even higher ones may be reached with a proper passivation scheme.

SUPPLEMENTARY MATERIAL

See the supplementary material for RHEED patterns and AFM pictures recorded for ScAlN films grown at different temperatures.

ACKNOWLEDGMENTS

This work has been carried out in the framework of the European Project GaN4AP (Gallium Nitride for Advanced Power Applications). The project has received funding from the Electronic Component Systems for European Leadership Joint Undertaking (ECSEL JU), under Grant Agreement No. 101007310. This Joint Undertaking receives support from the European Union's Horizon 2020 research and innovation program, and Italy, Germany, France, Poland, the Czech Republic, and the Netherlands. It was also supported by the French National Research Agency (ANR) through the "Investissements d'Avenir" program GaNeX (Grant No. ANR-11-LABX-0014) and the French technology facility network RENATECH.

AUTHOR DECLARATIONS

Conflict of Interest

The authors have no conflicts to disclose.

AUTHOR CONTRIBUTIONS

Caroline Elias: Formal analysis (equal); Investigation (equal); Writing – original draft (equal). **Maud Nemoz**: Formal analysis (equal). **Hélène Rotella**: Formal analysis (equal). **Frédéric Georgi**: Formal analysis (equal). **Stéphane Vézian**: Formal analysis (equal). **Maxime Hugues**: Formal analysis (equal); Investigation (equal); Writing – original draft (equal). **Yvon Cordier**: Conceptualization (lead); Funding acquisition (lead); Investigation (equal); Project administration (lead); Resources (lead); Supervision (lead); Writing – original draft (equal).

DATA AVAILABILITY

The data that support the findings of this study are available from the corresponding author upon reasonable request.

REFERENCES

[1] U. Strauß, A. Avramescu, T. Lermer, D. Queren, A. Gomez-Iglesias, C. Eichler, J. Müller, G. Brüderl, and S. Lutgen, Phys. Status Solidi B **248**, 652 (2011).
[2] M. Kneissl, T.-Y. Seong, J. Han, and H. Amano, Nat. Photonics **13**, 233 (2019).
[3] Y. Narukawa, M. Ichikawa, D. Sanga, M. Sano, and T. Mukai, J. Phys. D: Appl. Phys. **43**, 354002 (2010).
[4] F. Roccaforte and M. Leszczynski, *Nitride Semiconductor Technology: Power Electronics and Optoelectronic Devices* (Wiley-VCH, Weinheim, Germany, 2020).
[5] M. Meneghini, C. De Santi, I. Abid, M. Buffolo, M. Cioni, R. A. Khadar, L. Nela, N. Zagni, A. Chini, F. Medjdoub, G. Meneghesso, G. Verzellesi, E. Zanoni, and E. Matioli, J. Appl. Phys. **130**, 181101 (2021).
[6] J. P. Ibbetson, P. T. Fini, K. D. Ness, S. P. DenBaars, J. S. Speck, and U. K. Mishra, Appl. Phys. Lett. **77**, 250 (2000).
[7] O. Ambacher, B. Christian, M. Yassine, M. Baeumler, S. Leone, and R. Quay, J. Appl. Phys. **129**, 204501 (2021).
[8] G. H. Jessen, R. C. Fitch, J. K. Gillespie, G. Via, A. Crespo, D. Langley, D. J. Denninghoff, M. Trejo, and E. R. Heller, IEEE Trans. Electron Devices **54**, 2589 (2007).
[9] M. Higashiwaki, N. Hirose, and T. Matsui, IEEE Electron Device Lett. **26**, 139 (2005).

[10]M. T. Hardy, B. P. Downey, N. Nepal, D. F. Storm, D. S. Katzer, and D. J. Meyer, Appl. Phys. Lett. **110**, 162104 (2017).
[11]T. E. Kazior, E. M. Chumbes, B. Schultz, J. Logan, D. J. Meyer, and M. T. Hardy, in *IEEE MTT-S International Microwave Symposium (IMS)* (IEEE, 2019), pp. 1136–1139.
[12]M. A. Moram and S. Zhang, J. Mater. Chem. Mater. A **2**, 6042 (2014).
[13]M. A. Caro, S. Zhang, T. Riekkinen, M. Ylilammi, M. A. Moram, O. Lopez-Acevedo, J. Molarius, and T. Laurila, "Piezoelectric Coefficients and Spontaneous Polarization of ScAlN," J. Phys.: Condens. Matter **27**, 245901 (2015) (n.d.).
[14]J. Kuzmik, IEEE Electron Device Lett. **22**(11), 510 (2001).
[15]M. T. Hardy, E. N. Jin, N. Nepal, D. S. Katzer, B. P. Downey, V. J. Gokhale, D. F. Storm, and D. J. Meyer, Appl. Phys. Express **13**, 065509 (2020).
[16]J. Casamento, C. S. Chang, Y. T. Shao, J. Wright, D. A. Muller, H. Xing Grace, and D. Jena, Appl. Phys. Lett. **117**, 112101 (2020).
[17]P. Wang, D. Wang, B. Wang, S. Mohanty, S. Diez, Y. Wu, Y. Sun, E. Ahmadi, and Z. Mi, Appl. Phys. Lett. **119**, 082101 (2021).
[18]C. Manz, S. Leone, L. Kirste, J. Ligl, K. Frei, T. Fuchs, M. Prescher, P. Waltereit, M. A. Verheijen, A. Graff, M. Simon-Najasek, F. Altmann, M. Fiederle, and O. Ambacher, Semicond. Sci. Technol. **36**, 034003 (2021).
[19]S. Leone, J. Ligl, C. Manz, L. Kirste, T. Fuchs, H. Menner, M. Prescher, J. Wiegert, A. Žukauskaitė, R. Quay, and O. Ambacher, Phys. Status Solidi RRL **14**, 1900535 (2020).
[20]I. Streicher, S. Leone, L. Kirste, C. Manz, P. Straňák, M. Prescher, P. Waltereit, M. Mikulla, R. Quay, and O. Ambacher, Phys. Status Solidi RRL **17**, 2200387 (2022).
[21]A. J. Green, N. Moser, N. C. Miller, K. J. Liddy, M. Lindquist, M. Elliot, J. K. Gillespie, R. C. Fitch, R. Gilbert, D. E. Walker, E. Werner, A. Crespo, E. Beam, A. Xie, C. Lee, Y. Cao, and K. D. Chabak, IEEE Electron Device Lett. **41**, 1181 (2020).
[22]S. Krause, I. Streicher, P. Waltereit, L. Kirste, P. Brückner, B. Brückner, and S. Leone, IEEE Electron Device Lett **44**(1), 17 (2023).
[23]D. Wang, P. Wang, S. Mondal, S. Mohanty, T. Ma, E. Ahmadi, and Z. Mi, Adv Electron Mater **8**, 2200005 (2022).
[24]R. Dargis, A. Clark, A. Ansari, Z. Hao, M. Park, D. G. Kim, R. Yanka, R. Hammond, M. Debnath, and R. Pelzel, Phys. Status Solidi A **217**, 1900813 (2020).
[25]Y. Cordier, J.-C. Moreno, N. Baron, E. Frayssinet, S. Chenot, B. Damilano, and F. Semond, IEEE Electron Device Lett. **29**, 1187 (2008).
[26]P. Altuntas, F. Lecourt, A. Cutivet, N. Defrance, E. Okada, M. Lesecq, S. Rennesson, A. Agboton, Y. Cordier, V. Hoel, and J.-C. de Jaeger, IEEE Electron Device Lett. **36**, 303 (2015).
[27]J.-C. Gerbedoen, A. Soltani, S. Joblot, J.-C. de Jaeger, C. Gaquiere, Y. Cordier, and F. Semond, IEEE Trans. Electron Devices **57**, 1497 (2010).
[28]Y. Cordier, F. Pruvost, F. Semond, J. Massies, M. Leroux, P. Lorenzini, and C. Chaix, Phys. Status Solidi C **3**, 2325–2328(2006).
[29]Y. Cordier, F. Natali, M. Chmielowska, M. Leroux, C. Chaix, and P. Bouchaib, Phys. Status Solidi C **9**, 523 (2012).
[30]M. Björck and G. Andersson, J. Appl. Crystallogr. **40**, 1174 (2007).
[31]P. Wang, D. A. Laleyan, A. Pandey, Y. Sun, and Z. Mi, Appl. Phys. Lett. **116** (2020).
[32]S. Zhang, W. Y. Fu, D. Holec, C. J. Humphreys, and M. A. Moram, J. Appl. Phys. **114**, 243516 (2013).
[33]H. Kim-Chauveau, E. Frayssinet, B. Damilano, P. de Mierry, L. Bodiou, L. Nguyen, P. Vennéguès, J.-M. Chauveau, Y. Cordier, J. Y. Duboz, R. Charash, A. Vajpeyi, J.-M. Lamy, M. Akhter, P. P. Maaskant, B. Corbett, A. Hangleiter, and A. Wieck, J. Cryst. Growth **338**, 20 (2012).